

Article

Silver Nanoprism-Loaded Eggshell Membrane: A Facile Platform for In Situ SERS Monitoring of Catalytic Reactions

Yaling Li ¹, Yong Ye ¹, Yunde Fan ¹, Ji Zhou ^{1,*}, Li Jia ¹, Bin Tang ^{2,3,*} and Xungai Wang ^{2,3}

¹ Hubei Collaborative Innovation Center for Advanced Organic Chemical Materials & Key Laboratory for the Synthesis and Application of Organic Functional Molecules, Ministry of Education & College of Chemistry & Chemical Engineering, Hubei University, Wuhan 430062, China; liyaling@stu.hubu.edu.cn (Y.L.); yeyong@hubu.edu.cn (Y.Y.); vander@stu.hubu.edu.cn (Y.F.); jiali@hubu.edu.cn (L.J.)

² National Engineering Laboratory for Advanced Yarn and Fabric Formation and Clean Production, Wuhan Textile University, Wuhan 430073, China; xungai.wang@deakin.edu.au

³ Institute for Frontier Materials, Deakin University, Geelong, Victoria 3216, Australia

* Correspondence: zhouji@hubu.edu.cn (J.Z.); bin.tang@deakin.edu.au (B.T.); Tel.: +86-27-88662747; Fax: +86-27-88663043

Academic Editor: Helmut Cölfen

Received: 27 December 2016; Accepted: 3 February 2017; Published: 18 February 2017

Abstract: We reported the fabrication of an in situ surface-enhanced Raman scattering (SERS) monitoring platform, comprised of a porous eggshell membrane (ESM) bioscaffold loaded with Ag nanoprism via an electrostatic self-assembly approach. The localized surface plasmon resonance (LSPR) property of silver nanoprism leads to the blue color of the treated ESMs. UV-vis diffuse reflectance spectroscopy, scanning electron microscope (SEM), X-ray diffraction (XRD) and X-ray photoelectron spectroscopy (XPS) measurements were employed to observe the microstructure and surface property of Ag nanoprisms on the ESMs. The silver nanoprism-loaded eggshell membrane (AgNP@ESM) exhibited strong catalytic activity for the reduction of 4-nitrophenol by sodium borohydride (NaBH₄) and it can be easily recovered and reused for more than six cycles. Significantly, the composites also display excellent SERS efficiency, allowing the in situ SERS monitoring of molecular transformation in heterogeneous catalysis. The results indicate that the AgNP@ESM biocomposite can achieve both SERS and catalytic functionalities simultaneously in a single entity with high performance, which promotes the potential applications of ESM modified with functional materials.

Keywords: eggshell membrane; silver nanoprism; catalysis; SERS

1. Introduction

Noble metal nanoparticles, including gold and silver nanoparticles, are currently of great interest for their distinctive plasmonic properties and extensive research attention in near-field related applications, such as surface-enhanced spectroscopy [1,2], biomedicine [3,4], photonics [5,6], and biosensing [7,8]. Recently, metal nanoparticle-based catalysis has become an increasing area of research [9,10]. Lots of catalytic systems for various reactions are being explored. In order to pursue more efficient catalysis, gaining insights into the reaction paths and kinetics of reacting systems is still an ongoing topic of great interest.

UV-vis absorption spectroscopy and surface-enhanced Raman scattering (SERS) spectroscopy are the commonly used techniques for in situ investigation of metal-catalyzed reactions [11–14]. UV-vis absorption spectroscopy can provide the reactant transformation information of the reacting systems conveniently and facilely. SERS possesses inherent advantages of high specificity, sensitivity, and

selectivity, which can obtain detailed fingerprint vibrational information of the reactant, and the final product as well as the unstable transient reaction intermediate. Therefore, SERS has become a versatile and powerful tool for real-time monitoring of metal-catalyzed reactions, even at the single-nanoparticle level [15].

Among noble metal nanoparticles, silver nanoparticles have attracted intensive attention due to their high SERS/catalytic performance, easy preparation and control over size and shape. Typically, silver nanoparticles with diameters less than 10 nm possess a large surface area to volume ratio which contributes to the strong catalytic activity. However, it is almost impossible to acquire high Raman enhancement of adsorbed molecules on these small nanoparticles. It seems that the single type of silver nanoparticles can hardly exhibit both excellent catalytic and SERS activity. Therefore, combining catalytically-responsive and SERS-active functionalities into an entire platform through suitable methods of core-shell [16], hybrid [17,18], alloy [19] or assembly [20] is the most popular strategy. However, it is difficult to achieve a balance between high catalytic efficiency and SERS enhancement, as the plasmonic near-field enhancement is distance-dependent and the surface coverage of catalytic nanoparticles (NPs) may also remarkably reduce the SERS enhancement. It is well known that the shape and size control of silver nanoparticles is significant because it determines their optical properties and thus their related application field. Silver nanoprisms possess numerous low coordination atoms on their edges and corners, which may provide abundant activation sites for breaking the chemical bonds in catalytic reactions [21,22]. Meanwhile, the near infrared (NIR) LSPR bands of silver nanoprisms do not notably overlap with the absorption bands of water and most fluorescent molecules, leading to real-time SERS monitoring in an aqueous environment.

In addition, nanocatalyst colloid suspensions are commonly undesirable for practical applications because of easy aggregation and difficulties in product separation and catalysts recycling. Immobilizing metal nanoparticles on/into a porous matrix is an effective route to maintaining their activity and stability, as well as their reusability. Many supports including filter paper [23], cellulosic fibers [24], and polymer hydrogel [25] for the immobilization of nanoparticles have been already explored. Recently, natural biomass materials such as eggshell membrane [26–28], plant tissue [29] and mushroom [30] as effective catalyst supports provide “green” platforms to the catalytic reaction. Generally, ESMs, together with eggshells, are disposed of as waste materials. Recently, ESMs have been widely investigated because they are a rich resource with fascinating structures. Utilizations based on ESMs have been developed in various fields, such as heavy metal ions adsorption [31], high-performance electrode materials [32], as a separator in supercapacitor [33,34], biosensing [35] and catalysis [26–28].

Herein, a functional ESM modified with silver nanoprisms was fabricated through a self-assembly process. The interwoven fibrous structure of natural ESMs offers a large surface area for immobilization of silver nanoprisms. In this biomass-based platform, integration of a sensitivity SERS activity with an excellent catalytic property was achieved. The catalytic feature and recyclability were investigated through studying the reduction of 4-nitrophenol (4-NP) into 4-aminophenol (4-AP) by UV-vis spectroscopy. Furthermore, the obtained AgNP@ESM composites were then utilized for real-time monitoring of the catalytic reaction process of 4-nitrothiophenol (4-NTP) to 4-aminothiophenol (4-ATP) by observing the fingerprint signals of the reactants and products using SERS technology.

2. Results and Discussion

2.1. Optical Properties of AgNPs

Figure 1 shows the UV-vis extinction spectrum of Ag nanoprism colloid. Three extinction bands centered at 330, 504 and 700 nm were seen in the extinction spectrum. They are characteristic LSPR bands of Ag nanoprisms, ascribed to out-of-plane quadrupole, in-plane quadrupole and in-plane dipole resonance modes, respectively, consistent with the results in our previous report [36].

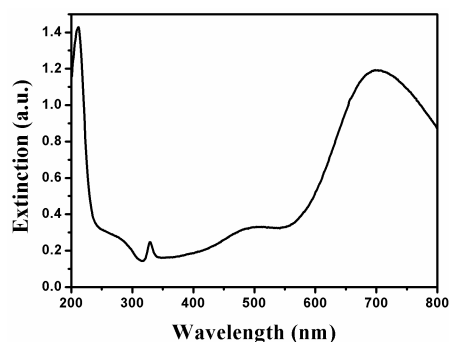


Figure 1. UV-vis extinction spectrum recorded for Ag triangular nanoprisms synthesized by the photoinduced conversion approach.

2.2. Characterization of AgNP@ESM Composites

ESM, as a natural semi-permeable membrane, is mainly composed of interwoven and coalescing nanofibers, and thus intrinsically possesses a large surface area. Thus, ESMs can be utilized as three-dimensional frameworks to load high density nanoparticles. In this study, PDDA was used to modify the surface property of ESM prior to treatment with AgNPs and then AgNPs were assembled on the ESM through electrostatic interaction between negatively charged AgNPs and positively charged PDDA modified ESM. SEM characterization was used to observe the morphologies of ESMs before and after treatment (Figure 2). The pristine ESM exhibited a three-dimensional grid-like structure, with a fibrous skeleton diameter ranging from 0.5 to 2.0 μm (Figure 2A,B). The hierarchically porous structure can endow ESM with good permeability, allowing reactants to contact the inner fibers sufficiently. After the assembly of AgNPs, the inherent interconnected fibrous structure of ESM was still preserved (Figure 2C). As can be seen from the SEM image with high magnification, lots of nanoparticles were immobilized on the surface of the fibrous structures of ESMs, dominated by triangular silver nanoplates (Figure 2D). The average sizes of AgNPs on the ESMs were measured as 58.5 ± 8.5 nm in edge length. The successful assembly of AgNPs on the ESMs also can be visually witnessed by the color change of ESM from white to blue. It is suggested that the color of the treated ESMs is generated from the LSPR optical feature of AgNPs. The result indicates that the assembly method based on electrostatic interaction is an effective route to realize a combination of ESMs and nanoparticles.

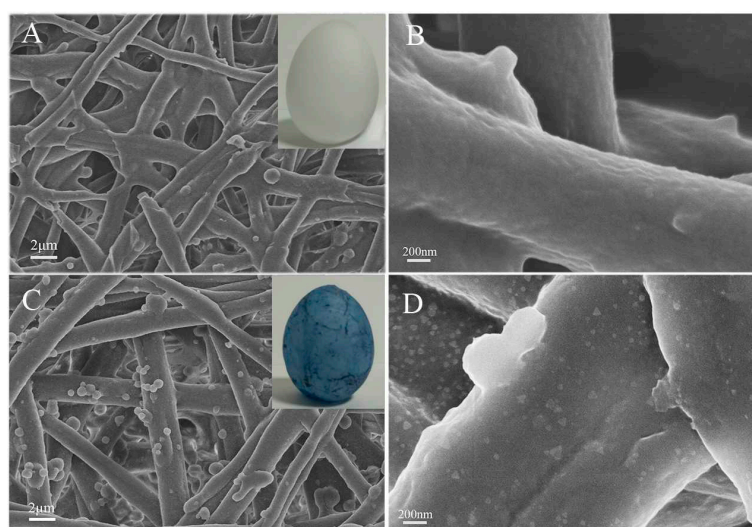


Figure 2. Scanning electron micrographs of pristine ESM (A,B) and the as-prepared AgNP@ESM composites (C,D) at different magnifications.

To further observe the optical properties of treated ESMs, UV-vis diffuse reflectance spectra were measured (Figure 3A). A small peak at 330 nm and a broad peak around 724 nm were observed, attributed to out-of-plane quadrupole and in-plane dipole LSPR bands of AgNPs. Compared with LSPR bands of AgNPs in solution, the in-plane dipole band of AgNPs on ESM red-shifted to 724 nm from 700 nm, which is due to the changes in the NPs' surroundings. Also, X-ray diffraction (XRD) measurement was performed to explore the crystal information of samples. The XRD patterns of ESM and AgNP@ESM are shown in Figure 3B. A visible peak corresponding to Ag (111) lattice plane confirms the presence of Ag (JCPDS 7440-22-4) on ESM. Moreover, the characteristic XRD peaks of ESM did not visibly change after the assembly of AgNPs, implying that crystal structures of ESM remained unchanged during treatment with silver nanoparticles.

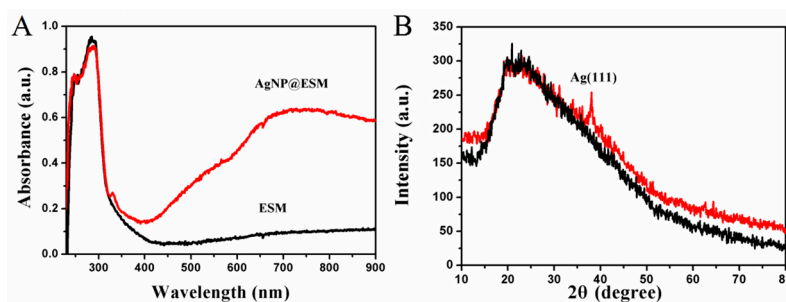


Figure 3. UV-vis diffuse reflectance spectra (A) and XRD pattern (B) of pristine ESM and AgNP@ESM.

Moreover, X-ray photoelectron spectroscopy (XPS) measurement was carried out to analyze the surface elements of ESMs after treatment with AgNPs. As shown in Figure 4, the survey scan spectrum of AgNP@ESM exhibits the presence of C 1s, N 1s, O 1s, Ag 3p, and Ag 3d core levels without significant impurities. In a high-resolution XPS spectrum (Figure 4B), two peaks were observed at 367.9 and 373.9 eV which are attributed to Ag 3d_{5/2} and Ag 3d_{3/2} of elemental silver. The splitting of the 3d doublet of Ag is 6.0 eV, indicating the presence of metallic Ag, which provides solid evidence for the assembly of AgNPs on the fiber surface [27].

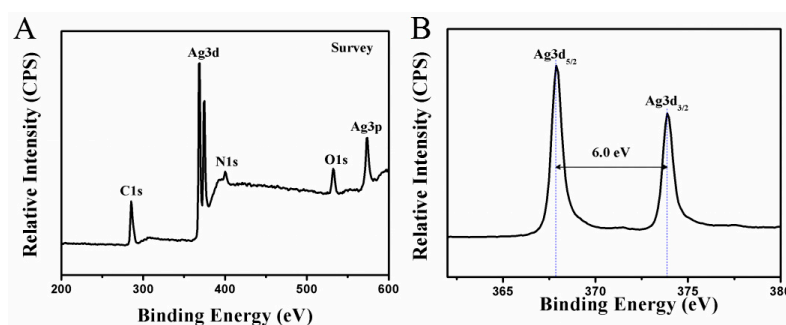


Figure 4. XPS spectra of AgNP@ESM composite: (A) survey; (B) Ag 3d.

2.3. Monitoring of the Catalytic Reaction with UV-vis

Ag nanoparticles have often been used to catalyze the reduction reactions involving nitrophenols, nitroanilines, and dyes [37,38]. In the present research, the interconnected porous structure of the ESMs is beneficial to the catalytic effect of AgNPs. Besides, the monolith piece of functional ESM is easily separated from the reaction system. ESMs not only provide a low-cost platform for immobilization of AgNPs, but also facilitate the separation and reuse of AgNPs after the catalytic reaction. The reduction of 4-NP by NaBH₄ was chosen as a model reaction to evaluate the catalytic activity of AgNP@ESM. Generally, the original 4-NP solution displays an absorbance peak at 317 nm, which shifts to 400 nm after adding NaBH₄ due to the formation of 4-nitrophenolate ions via deprotonation [39], with

color changes to yellow-green from light yellow. The UV-vis absorption spectra of 4-NP solution changed slightly in the presence of pristine ESM after 6 h (Figure 5A), revealing that the pristine ESM does not show catalytic activity for the reduction of 4-NP. However, the addition of AgNP@ESM led to the fading of the yellow-green color of the reaction mixture of 4-NP and NaBH₄ within 15 min. The absorption of the reaction solution containing 4-NP and NaBH₄ in the presence of AgNP@ESM was monitored with respect to time using UV-vis spectroscopy, and the resultant time-dependent evolution of the spectra is presented in Figure 5B. The intensity of the absorption peak at 400 nm decreased dramatically with reaction time, indicating the decrease of the initial reactant (4-NP). Meanwhile, a new absorption peak at approximately 300 nm appeared during this process, suggesting the generation of reduction product 4-AP [27,40]. Figure 5C displays the plot of the absorption intensity at 400 nm as a function of time corresponding to the treated ESMs. However, the absorption intensity corresponding to AgNP@ESM remained constant for a certain time and then decreased dramatically, implying that the AgNP@ESM exhibited remarkable catalytic activity for the reduction of 4-nitrophenol after an induction time [41]. In the presence of excess NaBH₄, the reduction of 4-NP is generally treated as a pseudo-first-order kinetic reaction [41,42]. Figure 5D shows the plot of $\ln(A_t/A_0)$ versus time. A_t and A_0 represent the absorption intensity at 400 nm at the time of t and the initial stage, respectively. It was observed that the reaction over this composite catalyst was almost complete within 800 s in the presence of NaBH₄. The linear correlation between $\ln(A_t/A_0)$ and time, as seen from Figure 5D, supports the pseudo-first-order assumption. The apparent rate constant (k_{app}) of the catalytic reactions can be obtained from the linear slope of $\ln(A_t/A_0)$ versus time. The k_{app} value of the reduction reaction was estimated to be $4.90 \times 10^{-3} \text{ s}^{-1}$. The k_{app} values obtained from AgNP@ESM are compared to the related results in literature for various matrix-supported AgNPs [24,26–28]. It is believed that good permeability of ESM can contribute to good catalytic property of AgNP@ESM, allowing reactants to contact with the active surface of Ag nanoprism sufficiently.

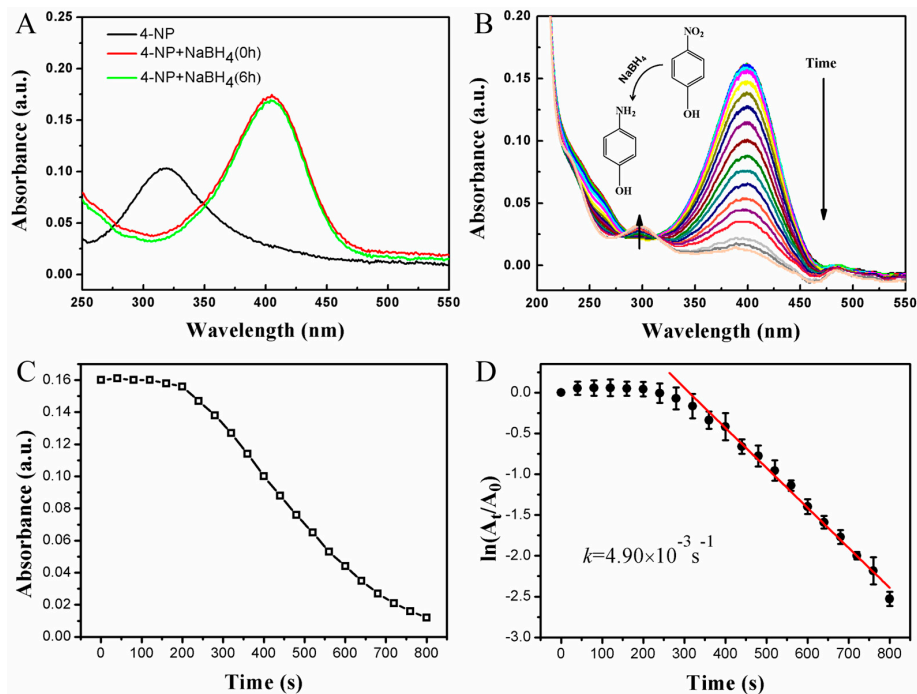


Figure 5. (A) The UV-vis absorption spectra of 4-NP solution before and after adding NaBH₄ 6 h with pristine ESM. (B) Evolution of the UV-vis absorption spectra of 4-NP solution with AgNP@ESM after NaBH₄ solution was added. (C) Plot of absorption intensity of 4-NP (400 nm) as a function of reaction time corresponding to AgNP@ESM. (D) Plot of $\ln(A_t/A_0)$ of the absorption peak at 400 nm versus time in the presence of AgNP@ESM. The $\ln(A_t/A_0)$ are averages of five measurements from different AgNP@ESMs and the error bars represent the standard error of these measurements.

In order to evaluate the reusability of the catalyst, the AgNP@ESM was recovered and reused in repeated reduction reactions of 4-NP. A_t/A_0 versus reaction time for each complete conversion was plotted in Figure 6. It is found that the AgNP@ESM still exhibit good catalytic activity even after six cycles. These results demonstrate that the AgNP@ESM biocomposites possess strong catalytic activity and good durability.

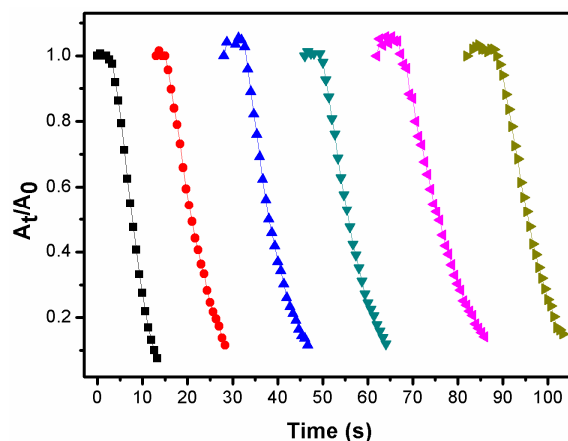


Figure 6. Recycling and reuse of AgNP@ESM for the reduction of 4-NP to 4-AP.

2.4. In Situ Monitoring of Catalytic Reaction with SERS

In addition to the catalytic properties of AgNP@ESM, we further explored its performance in SERS. We intended to use AgNP@ESM as a catalytic SERS platform for the real-time monitoring of chemical reactions that occur on their surface. The conversion of 4-nitrothiophenol (4-NTP) into 4-aminothiophenol (4-ATP) was selected as a model reaction, in which the thiol groups drive the chemisorption of the molecule on the surface of AgNPs through a strong Ag–S bond (see Figure 7A). Firstly, we put the treated ESMs into the solution of 4-NTP and left them for a certain period of time to allow a self-assembled monolayer of 4-NTP to adsorb on the surface of AgNPs, then the membrane was taken out and the residual 4-NTP molecules were washed out. Finally, the reduction of 4-NTP into 4-ATP was followed by real-time SERS after dropping a NaBH₄ solution on the membrane. Figure 7B shows the time-dependent SERS spectra of the 4-NTP-functionalized AgNP@ESM, which was recorded continuously for 270 s. The SERS spectra of 4-NTP exhibit four main characteristic peaks at 853, 1079, 1331 and 1568 cm⁻¹, attributed to C–H wagging, C–S stretching, O–N–O stretching, and phenyl ring stretching modes, respectively [19]. As the reaction progresses, new vibration Raman bands of an intermediate were observed 30 s later upon NaBH₄ addition, which can be assigned to the spectral features of 4,4′-dimercaptoazobenzene (4,4′-DMAB) at 1138, 1384, and 1428 cm⁻¹, ascribed to C–N symmetric stretching, N=N stretching and CH in-plane bending modes, respectively [16,19,43]. Meanwhile, the strong peaks at 853, 1331 and 1568 cm⁻¹, which correspond to R–NO₂ of 4-NTP, gradually decrease. After 120 s, the intensity of the 4-NTP and 4,4′-DMAB bands decreased significantly and a new band at 1590 cm⁻¹ emerged, confirming the formation of 4-ATP. Thus, we propose that 4,4′-DMAB is generated in the catalytic reaction but was immediately reduced to 4-ATP by the reducing agent NaBH₄. In short, there is a sequential hydride reduction of 4-NTP to 4,4′-DMAB and finally to 4-ATP. During the reaction time, it should be noted that the slight decrease of the SERS signals may be due to the loss of the catalysts, but the vibrational SERS bands produced by the interfacial reaction can still be obtained. It should be re-emphasized that the AgNP@ESM can achieve both SERS and catalytic functionalities in a single entity with high performance.

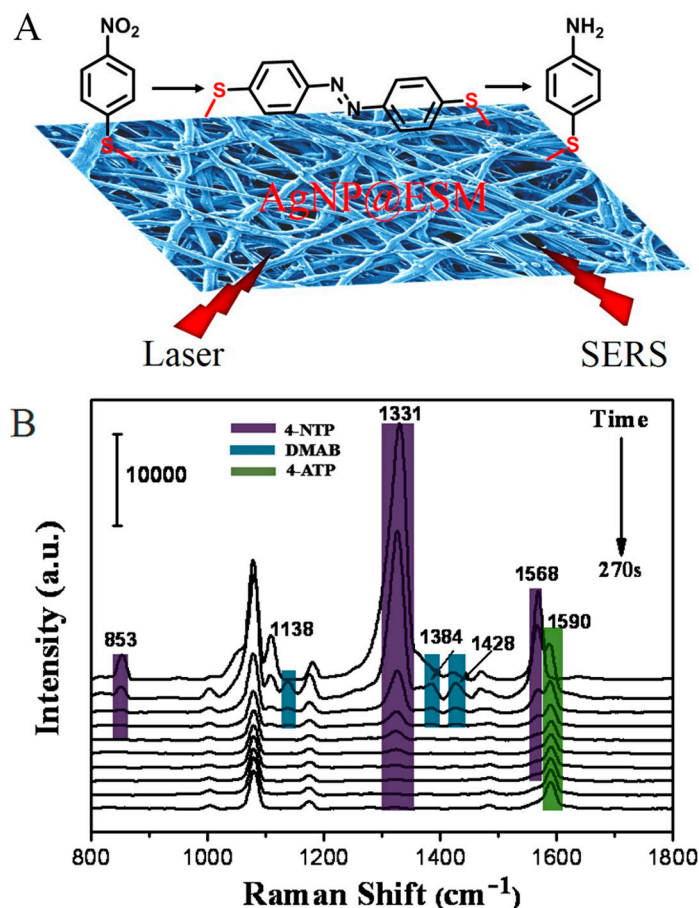


Figure 7. (A) Schematic illustration of 4-NTP conversion to 4-ATP on the AgNP@ESM surface and probing of the progress by SERS. (B) Time-dependent SERS spectra of 4-NTP conversion.

3. Materials and Methods

3.1. Materials

Silver nitrate (AgNO_3 , >99%), trisodium citrate ($\text{Na}_3\text{C}_6\text{H}_5\text{O}_7 \cdot 2\text{H}_2\text{O}$, $\geq 99.0\%$), sodium borohydride (NaBH_4 , >98%), 4-nitrophenol (4-NP, 99%), and 4-nitrothiophenol (4-NTP, 99%) were purchased from Aladdin Reagent Company (Shanghai, China). Poly(diallyldimethylammonium chloride) (PDDA, 20 wt %) was purchased from Sigma-Aldrich. All chemicals were of analytic grade, and used without further purification. Deionized water was obtained from Hangzhou Wahaha Co.

3.2. Characterization

Scanning electron microscopy (SEM) measurements were performed with a Hitachi S-4800 field emission SEM (Hitachi, Chiyoda, Japan). X-ray diffraction (XRD) patterns were recorded using a Bruker D8 Advance X-ray diffractometer (Bruker, Karlsruhe, Germany) with $\text{Cu K}\alpha$ radiation ($2\theta = 10^\circ\text{--}90^\circ$). X-ray photoelectron spectroscopy (XPS) measurements were carried out on a Kratos XSAM800 XPS system (Thermo Fisher, Waltham, MA, USA) with a $\text{K}\alpha$ source and a charge neutralizer. The ultraviolet-visible diffuse reflectance spectra (UV-vis DRS) of the as-prepared AgNP@ESM composites were obtained with an Ocean Optics USB4000 Spectrometer (Ocean Optics, Dunedin, FL, USA) and recorded with a reflection and backscattering probe. The UV-vis absorption spectra were obtained with an Ocean Optics USB4000 Spectrometer and recorded using Ocean Optics SpectraSuite software. The SERS analysis was performed on a Renishaw inVia Raman microscope system (Renishaw plc, Wotton-under-Edge, UK). A $50\times$ /N.A. 0.75 objective and a 785 nm high power diode laser

excitation source (>280 mW) were used in all measurements. The spectra within a Raman shift window between 800 and 1800 cm^{-1} were recorded using a mounted CCD camera with an integration time of 3 s through single scan.

3.3. Synthesis of Silver Nanoparticles

The silver nanoprisms were synthesized according to a photoinduced method. Briefly, an aqueous solution of AgNO_3 (0.1 mM, 100 mL) and trisodium citrate (100 mM, 1 mL) was mixed and vigorously stirred under ambient condition. NaBH_4 solution (8 mM, 1 mL) was then added dropwise into the mixing solutions. Yellow seed solutions were obtained and then irradiated under a sodium lamp (NAV-T 70 model from Osram China Lighting Co., Ltd.) for about 12 h. Finally, blue silver colloids were produced and kept in the dark at room temperature.

3.4. Fabrication of AgNP@ESM

Fresh eggs were obtained from a local supermarket. Raw eggshells were cleaned carefully with deionized water and broken gently. The inner yolk was removed and the ESM was carefully stripped from the raw egg and cleaned with deionized water. The clean white semipermeable ESMs were dried in air at ambient conditions, cut into small pieces ($3 \times 3 \text{ cm}^2$), and immersed in PDDA aqueous solution (2 wt %) for 2 h. Subsequently, the PDDA-ESMs were rinsed with abundant deionized water and then immersed in the silver nanoprism colloid. The weight ratio of colloid to ESM was 400:1. The solutions with ESMs were shaken for 3 h at 40 °C in an oscillating water bath. The ESM turned to blue from white, due to the assembly of Ag nanoprisms. Then, the AgNP@ESMs were rinsed with running deionized water and placed in glass Petri dishes and left for 24 h at room temperature in dark for drying.

3.5. Catalysis and SERS

To investigate the catalytic efficiency and reusability of the as-prepared AgNP@ESM, the catalytic reduction of 4-NP by NaBH_4 was performed according to our previously reported procedure. In a typical experiment, 2.0 mL of 4-NP aqueous solution ($1.0 \times 10^{-5} \text{ M}$) was put into a quartz cuvette with a path length of 1 cm. An amount of 3 mg of the AgNP@ESM was added to the 4-NP solution. Subsequently, 50 μL of freshly prepared NaBH_4 solution (0.6 M) was added to the mixed solution of 4-NP and AgNP@ESM under stirring. Meanwhile, the UV-vis absorption spectra were recorded. The parameters of the UV-vis absorption spectra were set as follows: integration time, 8 ms; scans to average, 10; boxcar width, 10; and interval, 8 s. The same composite membrane was used as a catalyst for at least six cycles.

To achieve in situ SERS monitoring, the conversion of 4-nitrothiophenol (4-NTP) into 4-aminothiophenol (4-ATP) was selected as another model reaction. The AgNP@ESM was immersed in $1.0 \times 10^{-5} \text{ M}$ 4-NTP ethanol solution for 1 h, and the 4-NTP molecules were arranged on silver surface as a result of surface crowding and strong Ag-S binding. Then, the membrane with 4-NTP was taken out, rinsed with ethanol and placed on a clean slide. An amount of 3 μL of NaBH_4 solution (0.3 M) was then dropped onto the composite membrane to initiate the reaction. The whole process was monitored by SERS spectroscopy, and each curve was recorded with an interval of 30 s. We collected the SERS spectra at different time points at an excitation of 785 nm and 1% of the laser output power.

4. Conclusions

In summary, we reported the preparation of a facile platform for the in situ SERS monitoring of catalytic reactions. In this low-cost platform, AgNPs were immobilized onto the eggshell membranes via electrostatic interaction. The pristine ESMs with an interwoven fibrous structure not only offer a large surface area for immobilization of AgNPs, but also feature good permeability that allows reactants to contact with the active surface of Ag nanoprism sufficiently. Moreover, the as-prepared AgNP@ESM also facilitates the separation and reuse of AgNPs catalysts. The treated ESMs exhibited

good catalytic activity and high reusability for the reduction of 4-NP. Furthermore, the application of the in situ SERS monitoring of the catalytic reduction of 4-NTP has been successfully carried out.

Acknowledgments: This research was supported by the National Natural Science Foundation of China (No. 51403162, 51273153) and the Educational Commission of Hubei Province of China (No. T201101). We also acknowledge support from the MoE Innovation Team Project in Biological Fibers Advanced Textile Processing and Clean Production (No. IRT13086).

Author Contributions: Ji Zhou and Bin Tang conceived and designed the experiments; Yaling Li and Yunde Fan performed the experiments; Yaling Li and Yong Ye analyzed the data; Li Jia contributed analysis tools; Yaling Li, Ji Zhou, Bin Tang and Xungai Wang wrote the paper.

Conflicts of Interest: The authors declare no conflict of interest.

References

1. Zaleski, S.; Wilson, A.J.; Mattei, M.; Chen, X.; Goubert, G.; Cardinal, M.F.; Willets, K.A.; Van Duyne, R.P. Investigating nanoscale electrochemistry with surface and tip-enhanced Raman spectroscopy. *Acc. Chem. Res.* **2016**, *49*, 2023–2030. [[CrossRef](#)] [[PubMed](#)]
2. Brown, L.V.; Yang, X.; Zhao, K.; Zheng, B.Y.; Nordlander, P.; Halas, N.J. Fan-shaped gold nanoantennas above reflective substrates for surface-enhanced infrared absorption (SEIRA). *Nano Lett.* **2015**, *15*, 1272–1280. [[CrossRef](#)] [[PubMed](#)]
3. Lim, W.Q.; Gao, Z. Plasmonic nanoparticles in biomedicine. *Nano Today* **2016**, *11*, 168–188. [[CrossRef](#)]
4. Teng, Z.; Zhang, J.; Li, W.; Zheng, Y.; Su, X.; Tang, Y.; Dang, M.; Tian, Y.; Yuwen, L.; Weng, L.; et al. Facile synthesis of yolk-shell-structured triple-hybridized periodic mesoporous organosilica nanoparticles for biomedicine. *Small* **2016**, *12*, 3550–3558. [[CrossRef](#)] [[PubMed](#)]
5. Li, Y.; Xin, H.; Liu, X.; Zhang, Y.; Lei, H.; Li, B. Trapping and detection of nanoparticles and cells using a parallel photonic nanojet array. *ACS Nano* **2016**, *10*, 5800–5808. [[CrossRef](#)] [[PubMed](#)]
6. Bose, S.; Sahoo, A.; Chattopadhyay, R.; Roy, S.; Bhadra, S.K.; Agrawal, G.P. Implications of a zero-nonlinearity wavelength in photonic crystal fibers doped with silver nanoparticles. *Phys. Rev. A* **2016**, *94*, 043835. [[CrossRef](#)]
7. Raymundo-Pereira, P.A.; Shimizu, F.M.; Coelho, D.; Piazzeta, M.H.O.; Gobbi, A.L.; Machado, S.A.S.; Oliveira, O.N. A nanostructured bifunctional platform for sensing of glucose biomarker in artificial saliva: Synergy in hybrid Pt/Au surfaces. *Biosens. Bioelectron.* **2016**, *86*, 369–376. [[CrossRef](#)] [[PubMed](#)]
8. Barsan, M.M.; Brett, C.M.A. Recent advances in layer-by-layer strategies for biosensors incorporating metal nanoparticles. *TrAC Trends Anal. Chem.* **2016**, *79*, 286–296. [[CrossRef](#)]
9. Oh, H.S.; Nong, H.N.; Reier, T.; Bergmann, A.; Gliech, M.; de Araujo, J.F.; Willinger, E.; Schlogl, R.; Teschner, D.; Strasser, P. Electrochemical catalyst-support effects and their stabilizing role for iron nanoparticle catalysts during the oxygen evolution reaction. *J. Am. Chem. Soc.* **2016**, *138*, 12552–12563. [[CrossRef](#)] [[PubMed](#)]
10. Oh, J.H.; Shin, H.; Choi, J.Y.; Jung, H.W.; Choi, Y.; Lee, J.S. In-plate and on-plate structural control of ultra-stable gold/silver bimetallic nanoplates as redox catalysts, nanobuilding blocks, and single-nanoparticle surface-enhanced Raman scattering probes. *ACS Appl. Mater. Interface* **2016**, *8*, 27140–27150. [[CrossRef](#)] [[PubMed](#)]
11. Atarod, M.; Nasrollahzadeh, M.; Sajadi, S.M. Euphorbia heterophylla leaf extract mediated green synthesis of Ag/TiO₂ nanocomposite and investigation of its excellent catalytic activity for reduction of variety of dyes in water. *J. Colloid Interface Sci.* **2016**, *462*, 272–279. [[CrossRef](#)] [[PubMed](#)]
12. Nasrollahzadeh, M.; Sajadi, S.M.; Hatamifard, A. Waste chicken eggshell as a natural valuable resource and environmentally benign support for biosynthesis of catalytically active Cu/eggshell, Fe₃O₄/eggshell and Cu/Fe₃O₄/eggshell nanocomposites. *Appl. Catal. B Environ.* **2016**, *191*, 209–227. [[CrossRef](#)]
13. Xie, W.; Walkenfort, B.; Schlucker, S. Label-free SERS monitoring of chemical reactions catalyzed by small gold nanoparticles using 3D plasmonic superstructures. *J. Am. Chem. Soc.* **2013**, *135*, 1657–1660. [[CrossRef](#)] [[PubMed](#)]
14. Zhang, J.; Winget, S.A.; Wu, Y.; Su, D.; Sun, X.; Xie, Z.X.; Qin, D. Ag@Au concave cuboctahedra: A unique probe for monitoring Au-catalyzed reduction and oxidation reactions by surface-enhanced Raman spectroscopy. *ACS Nano* **2016**, *10*, 2607–2616. [[CrossRef](#)] [[PubMed](#)]

15. Sambur, J.B.; Chen, P. Approaches to single-nanoparticle catalysis. *Annu. Rev. Phys. Chem.* **2014**, *65*, 395–422. [[CrossRef](#)] [[PubMed](#)]
16. Bao, Z.Y.; Lei, D.Y.; Jiang, R.; Liu, X.; Dai, J.; Wang, J.; Chan, H.L.; Tsang, Y.H. Bifunctional Au@Pt core-shell nanostructures for in situ monitoring of catalytic reactions by surface-enhanced Raman scattering spectroscopy. *Nanoscale* **2014**, *6*, 9063–9070. [[CrossRef](#)] [[PubMed](#)]
17. Jia, H.; Qiu, L.; Wang, J. A robust site-specific Au@SiO₂@AgPt nanorod/nanodots superstructure for in situ SERS monitoring of catalytic reactions. *RSC Adv.* **2015**, *5*, 40316–40323. [[CrossRef](#)]
18. Li, P.; Ma, B.; Yang, L.; Liu, J. Hybrid single nanoreactor for in situ SERS monitoring of plasmon-driven and small Au nanoparticles catalyzed reactions. *Chem. Commun.* **2015**, *51*, 11394–11397. [[CrossRef](#)] [[PubMed](#)]
19. Han, Q.; Zhang, C.; Gao, W.; Han, Z.; Liu, T.; Li, C.; Wang, Z.; He, E.; Zheng, H. Ag-Au alloy nanoparticles: Synthesis and in situ monitoring SERS of plasmonic catalysis. *Sens. Actuator B Chem.* **2016**, *231*, 609–614. [[CrossRef](#)]
20. Ding, Q.; Zhou, H.; Zhang, H.; Zhang, Y.; Wang, G.; Zhao, H. 3D Fe₃O₄@Au@Ag nanoflowers assembled magnetoplasmonic chains for in situ SERS monitoring of plasmon-assisted catalytic reactions. *J. Mater. Chem. A* **2016**, *4*, 8866–8874. [[CrossRef](#)]
21. Cui, Q.; Xia, B.; Mitzscherling, S.; Masic, A.; Li, L.; Bargheer, M.; Möhwald, H. Preparation of gold nanostars and their study in selective catalytic reactions. *Colloids Surf. A* **2015**, *465*, 20–25. [[CrossRef](#)]
22. Cui, Q.; Yashchenok, A.; Li, L.; Möhwald, H.; Bargheer, M. Mechanistic study on reduction reaction of nitro compounds catalyzed by gold nanoparticles using in situ SERS monitoring. *Colloids Surf. A* **2015**, *470*, 108–113. [[CrossRef](#)]
23. Zheng, G.; Polavarapu, L.; Liz-Marzan, L.M.; Pastoriza-Santos, I.; Perez-Juste, J. Gold nanoparticle-loaded filter paper: A recyclable dip-catalyst for real-time reaction monitoring by surface enhanced Raman scattering. *Chem. Commun.* **2015**, *51*, 4572–4575. [[CrossRef](#)] [[PubMed](#)]
24. Torkamani, F.; Azizian, S. Green and simple synthesis of Ag nanoparticles loaded onto cellulosic fiber as efficient and low-cost catalyst for reduction of 4-nitrophenol. *J. Mol. Liq.* **2016**, *214*, 270–275. [[CrossRef](#)]
25. Zhai, D.; Liu, B.; Shi, Y.; Pan, L.; Wang, Y.; Li, W.; Zhang, R.; Yu, G. Highly sensitive glucose sensor based on Pt nanoparticle/polyaniline hydrogel heterostructures. *ACS Nano* **2013**, *7*, 3540–3546. [[CrossRef](#)] [[PubMed](#)]
26. Liang, M.; Su, R.; Qi, W.; Yu, Y.; Wang, L.; He, Z. Synthesis of well-dispersed Ag nanoparticles on eggshell membrane for catalytic reduction of 4-nitrophenol. *J. Mater. Chem.* **2013**, *49*, 1639–1647. [[CrossRef](#)]
27. Liang, M.; Su, R.; Huang, R.; Qi, W.; Yu, Y.; Wang, L.; He, Z. Facile in situ synthesis of silver nanoparticles on procyanidin-grafted eggshell membrane and their catalytic properties. *ACS Appl. Mater. Interface* **2014**, *6*, 4638–4649. [[CrossRef](#)] [[PubMed](#)]
28. Mallampati, R.; Valiyaveetil, S. Eggshell membrane-supported recyclable catalytic noble metal nanoparticles for organic reactions. *ACS Sustain. Chem. Eng.* **2014**, *2*, 855–859. [[CrossRef](#)]
29. Sharma, N.C.; Sahi, S.V.; Nath, S.; Parsons, J.G.; Gardea-Torresde, J.L.; Pal, T. Synthesis of plant-mediated gold nanoparticles and catalytic role of biomatrix-embedded nanomaterials. *Environ. Sci. Technol.* **2007**, *41*, 5137–5142. [[CrossRef](#)] [[PubMed](#)]
30. Narayanan, K.B.; Park, H.H.; Han, S.S. Synthesis and characterization of biomatrixed-gold nanoparticles by the mushroom flammulina velutipes and its heterogeneous catalytic potential. *Chemosphere* **2015**, *141*, 169–175. [[CrossRef](#)] [[PubMed](#)]
31. Liu, B.; Huang, Y. Polyethyleneimine modified eggshell membrane as a novel biosorbent for adsorption and detoxification of Cr (VI) from water. *J. Mater. Chem.* **2011**, *21*, 17413. [[CrossRef](#)]
32. Chung, S.-H.; Manthiram, A. Carbonized eggshell membrane as a natural polysulfide reservoir for highly reversible Li-S batteries. *Adv. Mater.* **2014**, *26*, 1360–1365. [[CrossRef](#)] [[PubMed](#)]
33. Geng, J.; Wu, H.; Al-Enizi, A.M.; Elzatahry, A.A.; Zheng, G. Freestanding eggshell membrane-based electrodes for high-performance supercapacitors and oxygen evolution reaction. *Nanoscale* **2015**, *7*, 14378–14384. [[CrossRef](#)] [[PubMed](#)]
34. Yu, H.; Tang, Q.; Wu, J.; Lin, Y.; Fan, L.; Huang, M.; Lin, J.; Li, Y.; Yu, F. Using eggshell membrane as a separator in supercapacitor. *J. Power Sources* **2012**, *206*, 463–468. [[CrossRef](#)]
35. Xue, G.; Yue, Z.; Bing, Z.; Yiwei, T.; Xiuying, L.; Jianrong, L. Highly-sensitive organophosphorus pesticide biosensors based on CdTe quantum dots and bi-enzyme immobilized eggshell membranes. *Analyst* **2016**, *141*, 1105–1111. [[CrossRef](#)] [[PubMed](#)]

36. Tang, B.; Xu, S.; An, J.; Zhao, B.; Xu, W. Photoinduced shape conversion and reconstruction of silver nanoprisms. *J. Phys. Chem. C* **2009**, *113*, 7025–7030. [[CrossRef](#)]
37. Ghosh, S.K.; Kundu, S.; Mandal, M.; Pal, T. Silver and gold nanocluster catalyzed reduction of methylene blue by arsine in a micellar medium. *Langmuir* **2002**, *18*, 8756–8760. [[CrossRef](#)]
38. Herves, P.; Perez-Lorenzo, M.; Liz-Marzan, L.M.; Dzubiella, J.; Lu, Y.; Ballauff, M. Catalysis by metallic nanoparticles in aqueous solution: Model reactions. *Chem. Soc. Rev.* **2012**, *41*, 5577–5587. [[CrossRef](#)] [[PubMed](#)]
39. Muthuchamy, N.; Gopalan, A.; Lee, K.-P. A new facile strategy for higher loading of silver nanoparticles onto silica for efficient catalytic reduction of 4-nitrophenol. *RSC Adv.* **2015**, *5*, 76170–76181. [[CrossRef](#)]
40. Cloud, J.E.; Taylor, L.W.; Yang, Y. A simple and effective method for controllable synthesis of silver and silver oxide nanocrystals. *RSC Adv.* **2014**, *4*, 24551–24559. [[CrossRef](#)]
41. Tang, B.; Li, J.; Fan, L.; Wang, X. Facile synthesis of silver submicrospheres and their applications. *RSC Adv.* **2015**, *5*, 98293–98298. [[CrossRef](#)]
42. Ai, L.; Yue, H.; Jiang, J. Environmentally friendly light-driven synthesis of Ag nanoparticles in situ grown on magnetically separable biohydrogels as highly active and recyclable catalysts for 4-nitrophenol reduction. *J. Mater. Chem.* **2012**, *22*, 23447–23453. [[CrossRef](#)]
43. Van Schrojenstein Lantman, E.M.; Deckert-Gaudig, T.; Mank, A.J.G.; Deckert, V.; Weckhuysen, B.M. Catalytic processes monitored at the nanoscale with tip-enhanced Raman spectroscopy. *Nat. Nanotechnol.* **2012**, *7*, 583–586. [[CrossRef](#)] [[PubMed](#)]



© 2017 by the authors; licensee MDPI, Basel, Switzerland. This article is an open access article distributed under the terms and conditions of the Creative Commons Attribution (CC BY) license (<http://creativecommons.org/licenses/by/4.0/>).